Nat Hazards (2015) 77:2005–2026
DOI 10.1007/s11069-015-1689-7

ORIGINAL PAPER

Maximum-recorded overland run-ups of major nearfield paleotsunamis during the past 3000 years along the Cascadia margin, USA, and Canada

Curt D. Peterson[1] · Gary A. Carver[2] · John J. Clague[3] · Kenneth M. Cruikshank[1]

Received: 30 October 2014 / Accepted: 5 March 2015 / Published online: 1 April 2015

Abstract Maximum-recorded run-up estimates of six major nearfield paleotsunamis, dating from 0.3 to 2.8 ka, are compiled from reported studies at 12 reliable localities distributed over a north–south distance of 1000 km in the Cascadia subduction zone. The run-up estimates are based on surveyed elevations and positions of terminal sand sheet layers that were deposited by the dated paleotsunamis. Maximum terminal deposit elevations from open-coastal sites range from 3 to 12 m NAVD88. Paired proximal and distal run-up sites at four localities demonstrate landward vertical attenuation gradients (-2.5 to -4.2 m km^{-1}) of decreasing terminal sand deposit elevation with increasing distance inland. An averaged attenuation gradient is reversed (3.0 m km^{-1}) to project paleotsunami run-up elevations to adjacent ocean shorelines. The run-up projections are further adjusted by paleotsunami age and relative sea level curves to estimate shoreline inundation elevations under modern sea level conditions. The tsunami shoreline inundation elevations range from 3 ± 2 to 15 ± 2 m NAVD88, with the largest values occurring along the central Cascadia margin and the smallest values occurring in the eastern Juan de Fuca Strait. Contradictory to some numerical tsunami modeling assumptions, there is no apparent correlation between duration of interseismic strain accumulation or estimated upper-plate elastic flexure and corresponding paleotsunami run-up heights on the central Cascadia margin. The short duration since the last Cascadia megathrust rupture (0.3 ka)

✉ Curt D. Peterson
petersonc@pdx.edu

Gary A. Carver
cgeol@acsalaska.net

John J. Clague
jclague@sfu.ca

Kenneth M. Cruikshank
cruikshankk@pdx.edu

[1] Portland Sate University, PO Box 751, Portland, OR 97207-0751, USA

[2] Carver Geologic Inc., PO Box 52, Kodiak, AK 99615, USA

[3] Simon Fraser University, 8888 University Drive, Burnaby, BC V5A1S6, Canada

cannot be used to imply smaller run-up values for a near-future Cascadia tsunami. Coastal communities should plan for the maximum paleotsunami run-ups as recorded at the nearest reliable run-up localities.

Keywords Nearfield paleotsunami · Maximum run-ups · Cascadia subduction zone

1 Introduction

We compile reported measurements of maximum overland run-ups from major nearfield paleotsunamis along the Cascadia margin from southern Vancouver Island to northern California (Fig. 1). Major paleotsunamis in the study area are correlated with coastal coseismic subsidence events from megathrust ruptures of the central Cascadia subduction zone (Peterson et al. 2013a). Nearfield paleotsunami deposits (0.3–4 ka in age) occur widely along the Cascadia margin (Clague et al. 2000; Kelsey et al. 2005; Williams et al. 2005; Schlichting and Peterson 2006; Peters et al. 2007; Peterson et al. 2011). Although no major nearfield tsunamis have occurred along the Cascadia margin since European settlement, about 200 years ago, inundations from the last Cascadia paleotsunami in AD 1700 (Satake et al. 1996) are documented in oral traditions from Native American sources (Swan 1870; Andrade 1931; Sproat and Lillard 1987; Carver 1988; Ludwin et al. 2005; Phillips 2007; Younker 2007).

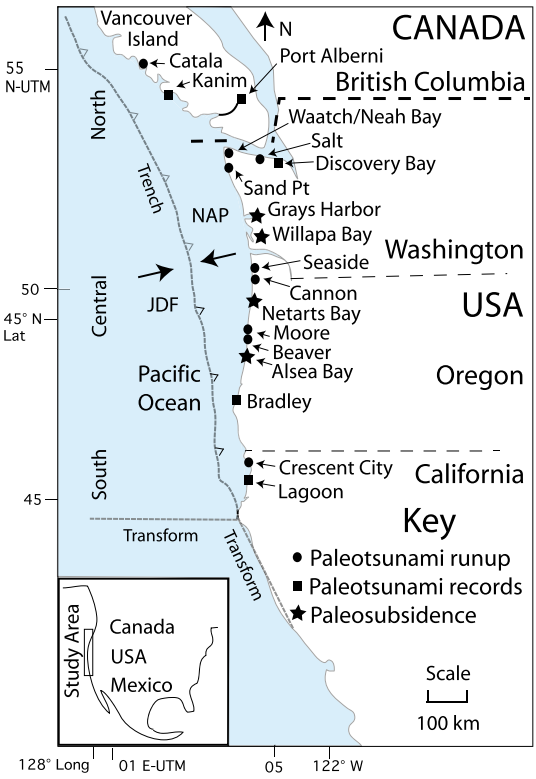

Fig. 1 Locations of major nearfield paleotsunami run-ups (*solid circles*), longer paleotsunami records (*solid squares*) and coseismic subsidence of tidal marshes (*solid stars*) along the Cascadia margin, as compiled in this study

A small subset of paleotsunami investigations (Osamu and Kenkyu 2007; Goff et al. 2012) has studies of the maximum landward extents of paleotsunami deposits to establish maximum heights and distances of recorded paleotsunami run-ups (Minoura and Nakaya 1991; Minoura et al. 2001; Peterson et al. 2008, 2011). In this paper, we compare previously documented sand deposit records of Cascadia paleotsunami run-ups to (1) positions along the margin (Fig. 1), (2) recurrence intervals between coastal coseismic subsidence events (Darienzo et al. 1994; Atwater et al. 2004) and (3) relative values of coseismic subsidence along the central margin (Shennan et al. 1996; Peterson et al. 2000; Peterson and Cruikshank 2014).

We utilize published paleotsunami run-ups in the Cascadia margin at 12 localities along the Cascadia margin, over a distance of about 1000 km (Fig. 1). In this study, the run-ups in the northern half of the margin are correlated with two rupture events with short preceding intervals. The smallest overland run-ups of major paleotsunamis along the central Cascadia margin correspond to the last megathrust rupture (AD 1700), which had a long recurrence interval and large estimated magnitude (M_w 9) (Adams 1996; Satake et al. 1996, 2003; Carver et al. 1999).

Analyses of Cascadia paleotsunami inundations during the past 3000 years demonstrate poor correspondence between event recurrence intervals and recorded maximum elevations of tsunami sand sheets. Uncertainties about the assumptions used in dislocation-fit modeling of tsunami excitation justify the use of paleotsunami run-up records to calibrate and/or independently verify modeled tsunami inundations along the Cascadia margin. The results from this study should have relevance to other subduction zones where uncertainties exist regarding the reliability of modeled tsunami excitations.

2 Background

Paleotsunami deposits that record overland inundations of tidal wetlands at the Cascadia margin include thin landward-thinning sheets of sand, and rarely gravel, bounded by mud and peat (Schlichting and Peterson 2006; Peters et al. 2007). Marine shell fragments and microfossils, including marine diatoms, have been used to confirm marine surge origins of these anomalous sand layers (Garrison-Laney; 1998; Hutchinson et al. 2000; Peterson and Cruikshank 2011). Beach gravel deposits that are draped over abandoned foredunes have also been interpreted to represent catastrophic marine surges from paleotsunamis along the Cascadia margin (Carver et al. 1998; Peterson et al. 2014). Beach sand deposits at substantial elevations ($\geq$7 m above mean sea level) and far from marine shorelines ($\geq$500 m landward distance) preclude origins from limited storm surge ($\leq$1.5 m height) and short-period storm wave inundations (Peterson et al. 2008). Paleotsunami sand sheets are distinguished by (1) beach sand mineralogy, (2) sharp bottom contacts, (3) upwards fining from fine sand to silt or sandy organics and (4) marine tracers, including shell fragments or marine microfossils (Hawkes et al. 2007; Goff et al. 2012).

In this study, we utilize published inundations of dated major nearfield paleotsunamis, as based on the landward distances and surveyed elevations of paleotsunami sand and/or gravel deposits ranging from 0.3 to 3.0 ka in age. The sand sheet deposits record the minimum run-ups of high-velocity flows that can transport coarse-grained sediment. The distinctive sand or gravel layers are preserved in stable lacustrine settings, barrage creek floodplain soils or abandoned foredune ridges. Due to the different paleotsunami mapping methods, deposit elevation surveying methods, and deposit age correlation methods used at

the different paleotsunami run-up localities (Fig. 1), we direct readers to the corresponding referenced articles for details about the specific methods and uncertainties used at each locality. The scope of this article is limited to analyses of (1) published terminal or maximum heights of paleotsunami sand sheet deposits, (2) along-margin positions of the run-up localities, (3) recurrence intervals of recorded coseismic subsidence events and (4) measured relative coseismic subsidence at localities positioned landward of the first zero-isobase, a proxy for corresponding elastic vertical seafloor displacements along the central Cascadia margin (Peterson and Cruikshank 2014).

Mapped paleotsunami inundations in tidal channels or coastal rivers are not used in this study due to uncertainties about tidal level and/or river stage impacts on inundations. Nor do we use overtopping estimates of paleotsunami run-up heights from prograding beach plains, active dune ridges or unstable beach sand ridges. We limited the period of record used in this study to the past 3 ka in order to (1) restrict run-up estimates to a period of minimal net sea level change and (2) obtain paleotsunami run-up data from events spanning at least two cycles each of short and long recurrence intervals between megathrust rupture events, as established from regional coseismic subsidence records (Table 1; Peterson et al. 2013a, b, 2014).

The constraints on suitable paleotsunami run-up settings outlined above limit the number of localities that we use to 12 (Fig. 1). Further, our constraint of deposit age ($\leq$3 ka) limits the number of events to the last five to six major nearfield paleotsunamis at the Cascadia margin (Table 1). The small sample size precludes formal statistical analysis of earthquake and tsunami magnitudes. However, we test some general assumptions that have been made about relations between lengths of recurrence intervals between dated regional coseismic subsidence events, relative coseismic flexure of the upper plate and resulting nearfield tsunami excitation (Fig. 2). The magnitudes of upper-plate coseismic uplift (seaward of the first zero-isobase) and subsidence (landward of the first zero-isobase)

Table 1 Cascadia major rupture coseismic subsidence events, ages, recurrence intervals and estimated subsidence in Washington and Oregon during the last 3 ka

Rupture event # (letter)	Age (ka)	Recurrence interval (year)	Coseismic subsidence Waatch (m)	Coseismic subsidence Willapa/GH (m)	Coseismic subsidence Netarts (m)	Coseismic subsidence Alsea (m)
1 (Y)	0.3	800	0.5	1.5	1.0	0.5
2 (W)	~1.1	200	0.5	1.0	0.5	0.5
3 (U)	~1.3	400	0.5	0.5	0.5	0.5
4 (S)	~1.7	1100		1.5	1.0	0.5
5 (N)	~2.6	200		0.5	0.5	
6 (L)	~2.8	400		1.0	0.5	
7 (J)	~3.2					

Ages, recurrence intervals and subsidence magnitudes are shown for Waatch Creek valley, Willapa Bay, and Grays Harbor (GH), Washington, and Netarts and Bays, Oregon (Fig. 1) for the past six to seven coseismic subsidence events, as previously lettered for Willapa Bay (Atwater et al. 2004). These dated coseismic subsidence events correspond to major paleotsunami inundations (Peterson et al. 2013a). Subsidence estimates, rounded to the nearest 0.5 m, are from Waatch (Peterson et al. 2013b), Willapa Bay and Grays Harbor (Shennan et al. 1996; Atwater and Hemphill-Haley 1997; Peterson et al. 2000), Netarts Bay (Darienzo et al. 1994), and Alsea Bay (Peterson and Darienzo 1996). Subsidence values differ between events and between localities, depending on relative position to the first zero-isobase (Fig. 2)

partly control tsunami excitation. The oblique convergence of the central Cascadia coastline with the first zero-isobase yields different amounts of measured coseismic subsidence along the margin. We use coseismic subsidence measurements from key localities (Peterson et al. 2014) to test the assumption that tsunami magnitude is largely controlled by the apparent magnitude of upper-plate coseismic flexure.

We do not compare measured paleotsunami run-ups with modeled excitation scenarios (Priest et al. 2010), because such scenario modeling has yielded a large range of predictions of possible run-up heights (4–30 m; Ng et al. 1990; Whitmore 1993, 1994; Geist and Yoshioka 1996; Walsh et al. 2000; Priest et al. 2000, 2013; Geist 2005; Tsunami Pilot Study Working Group 2006; Uslu et al. 2007; Cherniawsky et al. 2007; Witter et al. 2013). Rather, in this article, we present independent empirical measures of tsunami risk based on the past 3000 years of paleotsunami inundation records along the Cascadia margin.

3 Results

3.1 Geologic records of maximum-recorded paleotsunami run-up

Paleotsunami deposits have been documented in barrage creek marshes at Crescent City, CA (Figs. 1, 3; Peterson et al. 2011). Wide beaches and a sandy inner shelf in the Crescent

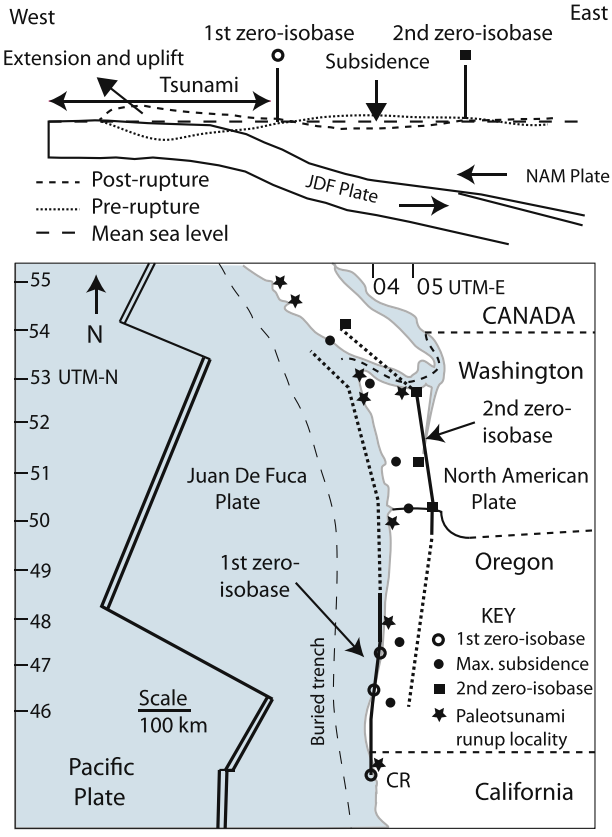

Fig. 2 Diagram and map of the first zero-isobase, second zero-isobase and maximum coseismic subsidence (Max.) of the North American plate based on elastic flexure models. Coseismic extension and uplift of the upper plate during megathrust rupture excite tsunamis (seaward and landward), with estimated nearfield tsunami landfall occurring 15–25 min after megathrust rupture. Paleotsunami run-up localities differ in distance from the mapped (*solid line*) and extrapolated (*dotted line*), first zero-isobase (Peterson and Cruikshank 2014)

City embayment (Peterson et al. 1991) provide ample sand supply for entrainment by catastrophic paleotsunami flows. Paleotsunami sand sheets in high-gradient creek wetlands have been correlated with rupture events 1–5 (Table 1) based on (1) radiocarbon ages from 152–429 to 2488–2920 cal yr BP and (2) similarity to paleotsunami sequences reported

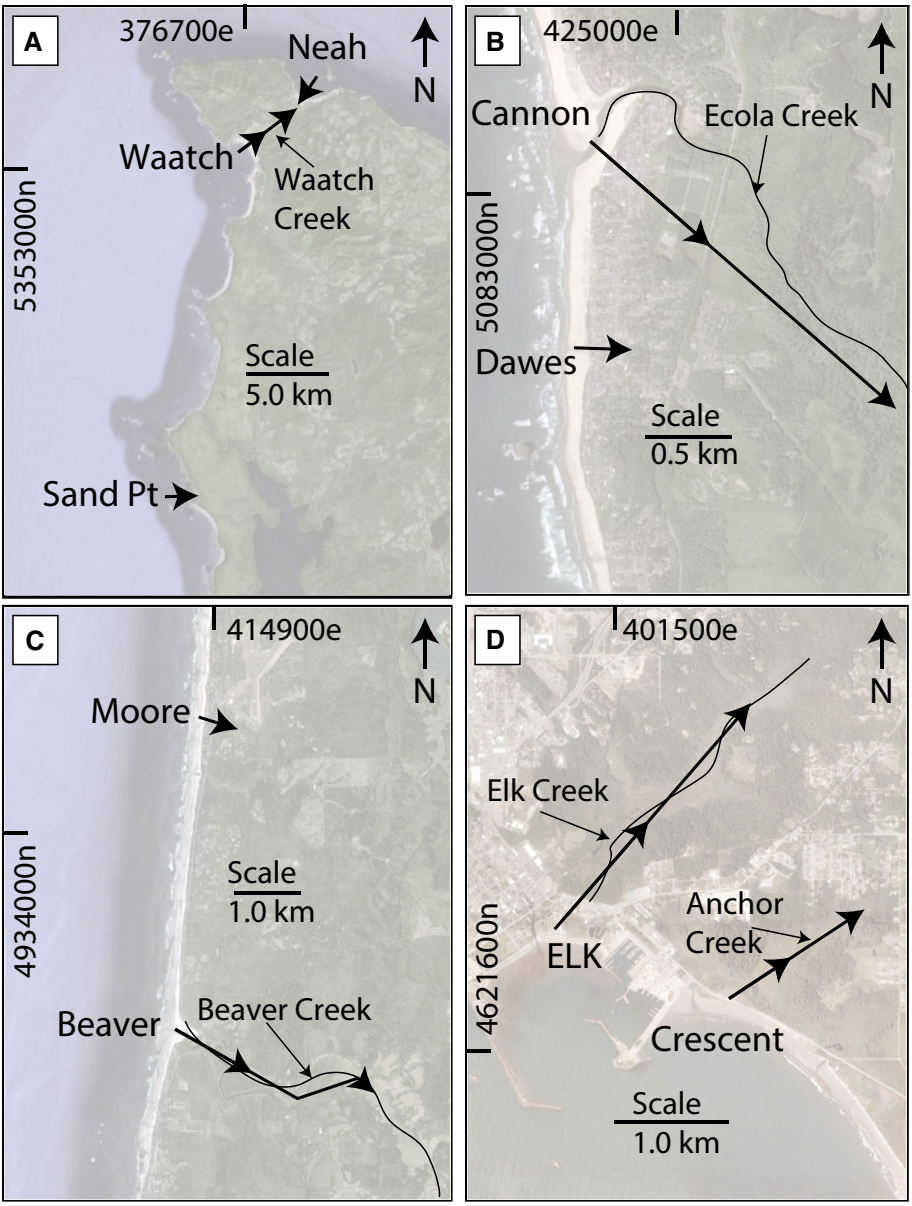

Fig. 3 Maps of paired paleotsunami run-up localites along the open coast. **a** Waatch/Neah/Sand Pt. in northernmost Washington. **b** Cannon/Dawes near the Washington–Oregon border. **c** Beaver/Moore on the central Oregon coast. **d** Elk/Crescent near the Oregon–California border. *Arrows* represent approximate paleotsunami run-up directions and distances based on extent of paleotsunami sand sheet deposits. See Fig. 1 for locations of paleotsunami run-up localities

Table 2 Paleotsunami run-up parameters

Locality	UTMn (m)	UTMe (m)	Event #/ age (ka)	Maximum distance (m)	Maximum elevation (m)	Shore run-up height (m)	*R*
Catala	5,522,800	639,700	#1/0.3	–	3*	4 ± 2	1
	5,522,800	639,700	#3/1.3	–	3*	4 ± 2	1
Kanim	5,475,000	693,200	#5/2.6	–	6*	4 ± 2	2
Neah	5,358,500	379,500	#1/0.3	–	6–7	7 ± 2	3
	5,358,500	379,500	#2a/0.9*	–	6–7	7 ± 2	3
	5,358,500	379,500	#2b/1.1	–	7–8	8 ± 2	3
	5,358,500	379,500	#3/1.3	–	≥8 ± 1	9 ± 2	3
Waatch	5,355,600	375,900	#1/0.3	2000	2.5	8 ± 2	3
	5,355,600	375,900	#2a/0.9*	2000	2.0	8 ± 2	3
	5,355,600	375,900	#2b/1.1	2500	2.0	9 ± 2	3
	5,355,600	375,900	#3/1.3	3000	2.5	12 ± 2	3
Sand Pt.	5,331,900	372,900	#3/1.3	–	9–10	11 ± 2	4
Salt	5,334,500	447,400	#4?/1.3–1.7	–	2–3	3 ± 2	5
	5,334,500	447,400	#5/2.6	–	2–3	3 ± 2	5
Cannon	5,083,000	425,200	#1/0.3	900	4.0	7 ± 2	6
	5,083,000	425,200	#2a/0.9*	1200	4.1	8 ± 2	6
	5,083,000	425,200	#2b/1.1	1200	3.9	8 ± 2	6
	5,083,000	425,200	#3/1.3	2100	6.5	14 ± 2	6
	5,083,000	425,200	#4/1.7	500	4.0	7 ± 2	6
Dawes	5,082,200	425,100	#3/1.3	300	10.7	14 ± 2	7
	5,082,200	425,100	#5/2.6	300	10.3	14 ± 2	7
Moore	4,936,000	415,000	#1/0.3	10	≤7.5	8 ± 2	7
	4,936,000	415,000	#3/1.3	450	12.3	15 ± 2	7
	4,936,000	415,000	#4/1.7	10	≤7.5	7 ± 2	7
	4,936,000	415,000	#5/2.6	450	12.0	15 ± 2	7
	4,936,000	415,000	#6/2.8–3.2	450	11.8	15 ± 2	7
Beaver	4,930,400	414,400	#1/0.3	2500	0	8 ± 2	8
	4,930,400	414,400	#2a/0.9*	750	0	3 ± 2	8
	4,930,400	414,400	#2b/1.1	1500	0	5 ± 2	8
	4,930,400	414,400	#3/1.3	4100	1.5	15 ± 2	8
	4,930,400	414,400	#4/1.7	1750	0	7 ± 2	8
	4,930,400	414,400	#5/2.6	4000	0.7	14 ± 2	8
Elk	4,622,800	401,100	#1/0.3	1100	3.0	6 ± 2	9
	4,622,800	401,100	#2/1.1	2500	4.0	13 ± 2	9

Table 2 continued

Locality	UTMn (m)	UTMe (m)	Event #/ age (ka)	Maximum distance (m)	Maximum elevation (m)	Shore run-up height (m)	*R*
Crescent	4,621,200	402,500	#1/0.3	400	5.5	7 ± 2	9
	4,621,200	402,500	#2/1.1	1200	8.6	13 ± 2	9
	4,621,200	402,500	#3/1.3	1200	8.2	13 ± 2	9
	4,621,200	402,500	#4/1.7	800	5.0	9 ± 2	9

UTM coordinates (m) are taken from the run-up locality shoreline. The following UTM sectors apply: Catala and Kanim Lakes (9U); Waatch, Neah, Salt Creek, and Sand Point (10U), all others (10T). Events are numbered 1–6 for nearfield paleotsunamis produced by central Cascadia megathrust ruptures (Table 1), except for event #2a (*), which has not been directly correlated with a central Cascadia megathrust coastal subsidence. Elevations (m) are in NAVD88, except at Catala and Kanim Lakes where mean sea level (MSL) is used. Maximum distance (m) is based on overland flow or flow in very shallow water (<1 m depth in seasonally flooded wetlands and small channels). Shoreline inundation height is estimated for the run-up locality at the paleoshoreline, based on (1) wave height attenuation gradient (3 m km^{-1}) with distance landward to terminal sand sheet deposits and (2) regional changes in paleosea level since the event age (Table 1). Paleosea level adjustments are based on (1) −1.0 m ka^{-1} relative sea level fall for Vancouver Island (Hutchinson et al. 2000; James et al. 2000), (2) +0.25 m ka^{-1} relative sea level rise for Salt Creek (Hutchinson et al. 2013) and (3) +0.75 m ka^{-1} relative sea level rise for all other localities in Washington, Oregon and California (Darienzo et al. 1994; Atwater and Hemphill-Haley 1997; Peterson et al. 2011). Run-up uncertainties of ±2 m are included to address uncertainties of possible storm surge (1.5 m) or extreme tidal range (4 m or ±2 m MSL) during paleotsunami events. Run-up data references (R) are as follows: (1)—Clague et al. (1999), (2)—Hutchinson et al. (1997); (3)—Peterson et al. (2013b), (4)—Peterson et al. (2014), (5)—Hutchinson et al. (2013), (6)—Peterson et al. (2008), (7)—Peterson and Cruikshank (2011), (8)—Peterson et al. (2009), (9)—Peterson et al. (2011)

from Lagoon Creek (Abramson 1998; Garrison-Laney 1998). Paleotsunami sand sheets corresponding to events 1–4 at Crescent City extend to an elevation of 3.8 m (NAVD88) 500 m from the present shoreline (event #1) to 8.2–8.6 m at a distance of 1200 m from the shoreline (events #2 and #3) in the Anchor Marsh Creek (Table 2). Overland run-up in the Elk Creek wetland at the north end of Crescent City (Fig. 3) reached an elevation of 3 m at a distance of 1100 m from the shoreline during event #1 and 4.0-m elevation at a distance of 2500 m from the shoreline (Table 2).

No reports of terminal overland paleotsunami deposition are available for southern Oregon; thus, there is a data gap along this portion of the Cascadia margin. Beach ridge overtopping from events #1–5 has been reported in Bradley Lake, OR (Fig. 1; Kelsey et al. 2005). However, the elevation of the paleobeach ridge that impounded Bradley Lake at the time of these events is not precisely known (its present elevation is 5–8 m). Furthermore, several disturbance layers in Bradley Lake were attributed to seismic shaking and not to beach ridge overtopping by paleotsunamis (Kelsey et al. 2005). Bradley Lake is not a suitable locality for establishing maximum overland run-up records, although it does demonstrate a continuity of paleotsunami inundations from rupture events #1–5 on the southern Oregon coast.

Paleotsunami sand sheet extents have been reported for paired localities on the central Oregon coastline, in the low-gradient Beaver Creek and the high-gradient Moore Creek (Fig. 3; Peterson et al. 2009; Peterson and Cruikshank 2011). Sandy beaches and a broad shallow sandy inner shelf provided an abundant supply of sand for paleotsunami entrainment at both localities (Peterson et al. 1991). Maximum extents of paleotsunami sand sheets along Beaver Creek range from 750 m from the present shoreline (event #2a at 0.8–0.9 ka) to 4000–4100 m for events #3 and #5 (Table 2). Paleotsunami event #2a has

not been found farther south of Beaver Creek along the central Cascadia margin (Peterson and Darienzo 1996). The large run-up distances for events #3 and #5 correspond to high run-up elevations (~12 m) at 450 m from the shoreline along the high-gradient Moore Creek. Thin (<0.5 cm) paleotsunami sand layers thought to record events #2 and #4 occur at the most seaward sites (7- to 8-m elevation) along Moore Creek.

Six overland inundation events dating back to 3080–3360 cal yr BP are recorded in the back-barrier Ecola Creek wetland at Cannon Beach (Peterson et al. 2008). The Cannon Beach locality includes a sandy inner shelf, broad beaches and a low (5- to 6-m elevation) barrier sand ridge (Fig. 3; Peterson et al. 1991), which provided abundant sand for paleotsunami entrainment. Paleotsunami events #1, #2a and #2b are radiocarbon dated at, respectively, 310–510, 910–1080 and 1060–1240 cal yr BP. Events #2a and #2b were initially thought to represent a single event, but subsequent dating separated the couplet into rupture event #2b at 1.1 ka and an earlier paleotsunami event #2a at 0.8–0.9 ka that was not accompanied by regional coseismic subsidence (Peterson et al. 2013a). The fourth paleotsunami layer (event #3) has been radiocarbon dated at 1276–1411 cal yr BP. Event #3 reached an elevation of 6.5 m at a distance of 2100 m from the ocean shoreline (Table 2). Shorter inundation distances (500–1200 m) and corresponding lower elevations (3.9–4.1 m) of paleotsunami terminal deposits are associated with events #1, 2a, 2b and 4 in the supratidal back-barrier wetlands at Ecola Creek.

Proximal sites Canu116 and Canu119 in the high-gradient Dawes Creek wetlands at the south end of Cannon Beach (Fig. 3) contain two paleotsunami sand layers (Peterson and

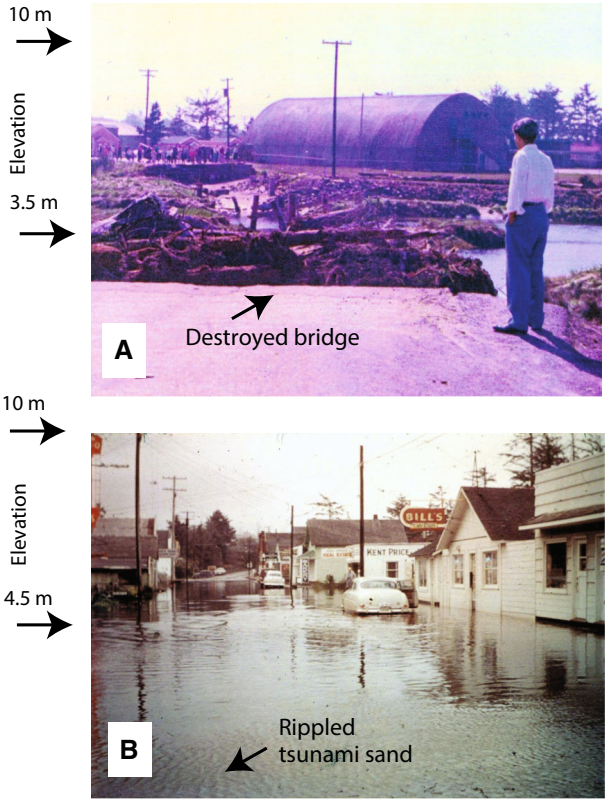

Fig. 4 **a** Destroyed Ecola Creek bridge (*arrow*) following the 1964 farfield tsunami. The historic tsunami run-up height at the bridge was at an elevation of 3.5 m NAVD88 (*arrow*). **b** Undrained water from tsunami inundation in 1964 on the landward side of the barrier beach ridge at an elevation of 4.5 m (*arrow*) in Cannon Beach. Corresponding paleotsunami run-up elevations are shown at 10-m elevation NAVD88 (*arrows*) for the two sites. The 10-m run-up elevations are based on paleotsunami sand sheets (events #3 and #5) reaching 10-m elevation at an inland distance of 300 m from the shoreline at Dawes Creek (Fig. 3; Table 2). Historic photographs are from Cannon Beach Historical Society, Cannon Beach, OR

Cruikshank 2011). The two largest events of paleotsunami run-up in nearby Seaside, Oregon (Fig. 1) correspond to dated deposits at 1060–1260 (event #3) and 2780–2950 (event #5 or #6) (Peterson et al. 2010). The paleotsunami layers at Canu119 are assigned to events #3 (1060–1260 cal yr BP) and event #5 (2780–2950 cal yr BP), at 10.7- and 10.3-m elevation, respectively, at a landward distance of 300 m from the ocean shoreline (Peterson et al. 2010).

Cannon Beach and Seaside, OR, along with Crescent City, CA, and Port Alberni, BC (Fig. 1) received significant damage from a farfield historic tsunami in 1964. That tsunami originated in the Gulf of Alaska from a great subduction zone earthquake (M_w 9.2). The maximum elevations reached by the tsunami at Cannon Beach were 4.5–5.0 m at the barrier beach ridge and 3.5–4.0 m in the back-barrier wetlands (Landers et al. 1993; Peterson et al. 2013a). The tsunami destroyed the Ecola Creek bridge, but left most of the wood-framed buildings in Cannon Beach intact (Fig. 4). In comparison, the paleotsunami deposits from nearfield Cascadia events #3 (1.3 ka) and #5 (2.6 ka) at the Dawes Creek locality in Cannon Beach (Fig. 3) extend up to 10-m elevation (Table 2). Both the Ecola Creek bridge site and the paleotsunami sand sheet deposits in the Dawes Creek wetland are located about 300-m inland from the present shoreline. A 10-m-high tsunami surge at 300 m distance from the shoreline, had it occurred in 1964, would not have left a single unreinforced building standing on either the barrier beach ridge or the back-barrier flats in Cannon Beach.

Another maximum run-up data gap exists along the south-central Washington coast. Prograded Holocene beach plains and barrier spits, 1–3 km wide, at Grays Harbor and Willapa Bay (Fig. 1) do not provide stable shoreline positions for evaluating past maximum paleotsunami run-up distances. Minimum inundation distances of 500, 1000, 1200, 1500, respectively, have been reported for events #1, #2a, #2b and #3 on the Willapa Bay sand spit, which has an elevation range of 4- to 7-m elevation (Schlichting and Peterson 2006). Although maximum paleotsunami run-ups cannot be established on these prograded beach plains, the geologic evidence of paleotsunami sand sheet deposition demonstrates the continuity of major paleotsunami inundation events #1–3 along the south-central Washington coast.

Four paleotsunami sand sheet layers are present in peaty mud wetland soils of the Waatch Creek valley in northwest Washington (Figs. 1, 3; Peterson et al. 2013b). Wide beaches and a beach sand barrier $\sim$250 m wide at the mouth of Waatch Creek provide abundant sand for paleotsunami entrainment. The oldest of the four paleotsunamis (event #3) was radiocarbon dated at 1260–1330 cal yr BP. At least three of the four paleotsunami sand sheets were associated with coseismic subsidence, although amounts of subsidence were small (Table 1). Maximum elevations of the paleotsunami sand sheets in the Waatch Creek wetland range from 2.5 m at a distance of 3200 m from the shoreline (event #1) to 2.5 m at a distance of 4600 m from the shoreline (event #3) (Table 2). The Waatch Creek wetland is an in-filled lagoon that extended about 1300 m landward from the modern shoreline in latest prehistoric time; thus, the overland inundation distances of paleotsunami events #1–3 are taken to be 1300 m less than the measured distance to the present shoreline at the modern mouth of Waatch Creek (Peterson et al. 2013b).

Based on the large inundation distance of paleotsunami event #3 in the Waatch Creek wetland, we searched for evidence of proximal run-up at the ocean shoreline. Although we found no suitable sites near the mouth of Waatch Creek, an anomalous gravel layer overlies an abandoned foredune ridge just north of Sand Point (Peterson et al. 2014; Fig. 3). The fine gravel layer is 5–30 cm thick and extends to a maximum elevation of 9.0 m at 80 m landward distance from the shoreline (Table 2). The abandoned foredune

sand ridge occurs about one-third of the distance across the prograded gravelly sand beach plain, dated from 1.5 to 0.6 ka. We tentatively attribute the marine surge that deposited the gravel on top of the sand ridge to paleotsunami event #3 (Table 1). Lower anomalous gravel layers (4- to 7-m elevation) were found on the seaward side of the late Holocene beach plain (40–70 m shoreline distance), and they are possibly related to later paleotsunami events #1–2.

Paleotsunami run-up has been reported at two localities farther east on the Washington coast, at Neah Bay and Salt Creek, located at opposite ends of the Juan de Fuca Strait (Fig. 1). At Neah Bay, paleotsunami sand sheet deposits are locally preserved in back-barrier wetlands ~100 m inland of a 300-m-wide stable barrier beach ridge (Fig. 3; Peterson et al. 2013b). The peaty mud that hosts the sandy paleotsunami deposits dates from the modern surface back to 2340–2430 cal yr BP. The stable surface of the barrier ridge (6- to 8-m elevation) dates to 1876–2330 cal yr BP. One paleotsunami (event #3) overtopped the highest part of the barrier ridge at 8 m, whereas later paleotsunamis (events #1 and 2) overtopped only those parts of the ridge below 6- to 7-m elevation (Table 2). No

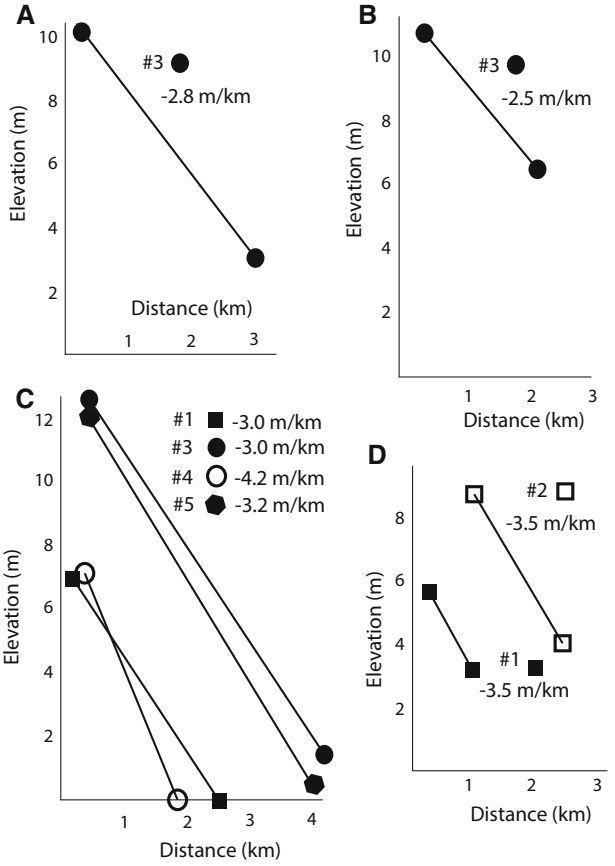

Fig. 5 Paleotsunami run-up attenuation gradients (two-point calibrations) based on extents of paleotsunami sand sheets, including maximum-recorded elevation (m NAVD88) and maximum landward distance (km) for corresponding events (#) at low-gradient (distal) and high-gradient (proximal) paired sites at four localities. Landward elevation attenuation gradients of terminal deposits range from −2.5 to −4.2 m km^{-1}, and average −3.2 m km^{-1}. Data are from Fig. 3 and Table 2

paleotsunami sand sheets were found in wetland soil deposits that predated the paleotsunami event #3 at ~1.3 ka and postdated the basal peat mud at 2.3–2.4 ka in the back-barrier wetlands of Neah Bay.

Two very thin paleotsunami sand sheets (~1 cm thick) are locally observed in tidal marsh deposits near the mouth of Salt Creek (Hutchinson et al. 2013). The two sand layers were attributed to paleotsunami inundations that covered the paleomarsh surface (2.0-m elevation at site 'a') but did not overtop the barrier beach ridge (250 m wide) at a present elevation of 3 m NAVD88. The deeper sand layer (0.7 m depth) is radiocarbon dated at 2360–2700, so it correlates with event #5 at 2.6 ka. The younger sand layer (0.6 m depth) is younger than a peat sample (0.65 m depth) dated at 1620–1820. The origin of the upper sand layer could be from either the rupture event #3 at 1.3 ka or the rupture event #4 at 1.7 ka (Table 1) depending on the age difference between the sand sheet layer and underlying dated peat sample.

Kanim Lake, located on the exposed outer west coast of Vancouver Island (Fig. 1), provides a long record of continuous mud deposition (0–4 ka) capable of hosting paleotsunami deposits (Hutchinson et al. 1997). The modern lake outlet lies at an elevation of 6 m at a distance of 300 m from the ocean shoreline. Only one thin paleotsunami sand layer, with marine diatoms, was found in the lake muds, and it returned an age of 2720–2840 cal yr BP. This paleotsunami likely corresponds to rupture event #5 (Table 1).

The northernmost paleotsunami run-up locality used in this study is Catala Lake, located on the open west coast of Vancouver Island (Fig. 1; Clague et al. 1999). At least two paleotsunamis inundated a shallow (1 m deep) outlet channel and the lake, 500 m inland from the ocean shore. Paleotsunami sand and gravel layers hosted within the lake muds dated to 360 ± 60 and 1350 ± 70 cal yr BP, and they are attributed to rupture events #1 at # 3 (Table 1). Clague et al. (1999) also identified an intervening paleotsunami layer, tentatively dated to ~1 ka, possibly event #2a or #2b in Catala Lake.

4 Discussion

4.1 Maximum-recorded major paleotsunami run-ups

Maximum-recorded elevations of major nearfield paleotsunami deposits (Peterson et al. 2013a) along the Cascadia margin are 8.6 m in Crescent City, CA; 12.3 m at Moore Creek, OR; 10.7 m at Cannon Beach, OR; and 9.0 m at Sand Point, WA (Fig. 3; Table 2). Overland inundations of the largest paleotsunamis, based on terminal sand sheet deposits, range from 2 to 4 km on low-gradient creek floodplains (1- to 6-m elevation). Previous studies of historic tsunamis show that (1) maximum inundation elevations can be 1–2 m greater than elevations of terminal sand sheet deposits in high-gradient creek valleys and (2) maximum inundation distances can exceed distances of terminal sand sheet deposits by several hundreds of meters in some low-gradient creek valleys (Peterson et al. 2011) and coastal plains (Goto et al. 2008). Given an abundant sand supply in beaches and the inner shelves of the selected run-up localities, the inland limits of sand sheets record the maximum elevations and distances that high-velocity flows ($\geq$1 m s^{-1} and $\geq$1 m flow depth) transported sand-size sediments over vegetated floodplain surfaces.

The highest paleotsunami deposits in proximal high-gradient creek valleys correspond to paleotsunami sand sheets farthest from the coast in distal low-gradient creek valleys at four paired localities in Washington, Oregon and California (Fig. 5). That is to say that the

highest paleotsunamis reached the furthest distance inland, so that the longer terminal inundation distances yielded lower terminal deposit elevations. We refer to the decrease in terminal deposit elevation with an increase in inundation distance as the landward run-up elevation attenuation gradient. We evaluated the landward elevation gradients of sand sheets for five different paleotsunami events at four of the paired localities. The landward elevation gradients range from -2.5 to -4.2 m km^{-1} for the five events. The average elevation gradient in the paired creek valleys ($N = 8$ samples) is -3.2 ± 0.5 m km^{-1}. For example, a terminal sand sheet deposit at 9-m elevation in a proximal shoreline site would decrease to $\sim$3-m elevation at a terminal landward distance of 2.0 km in a low-elevation distal site. Complex topographies from high beach ridges, substantially narrowing or widening creek valleys, and/or other flow impounding features might produce different elevation gradients of paleotsunami run-up based on preserved terminal sand sheet deposits.

4.2 Normalization of paleotsunami shoreline inundation elevations

We project paleotsunami inundation heights from terminal deposit positions to adjacent ocean shorelines in the four paired run-up localities based on a seaward run-up elevation gradient of 3.0 m km^{-1} (Fig. 5; Table 2). That is to say that we add 3.0 m of elevation height for every 1.0 km distance to the shoreline from the terminal paleotsunami deposit position. This normalization is done to compare the run-up proxy data between different sites and different events. To ensure that comparisons are uniform, we project all terminal paleotsunami deposit elevations, including those from proximal sites, to present beach shoreline positions. To compare paleotsunami shoreline inundation heights relative to different paleosea levels in the past 3 ka (Table 1), we adjust the projected shoreline inundation heights to the modern datum, 0 m NAVD88, or about -1-m mean sea level

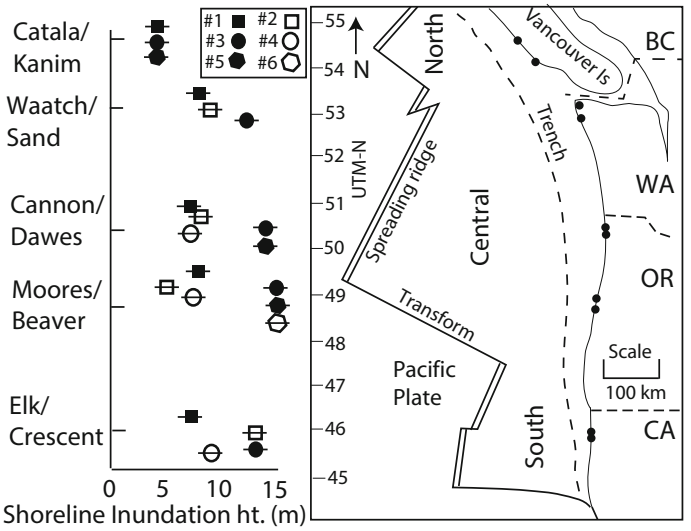

Fig. 6 Estimated shoreline inundation heights (±2 m NAVD88) for major nearfield paleotsunamis along the Cascadia margin over the past 3000 years. Ages of Cascadia rupture events and associated nearfield paleotsunamis are as follows: #1–0.3 ka; #2–1.1 ka; #3–1.3 ka; #4–1.7 ka; #5–2.6 ka; #6–2.8 ka (Tables 1, 2)

(MSL) using (1) the age of the paleotsunami event and (2) published relative sea level curves (Table 2). The estimated shoreline inundation heights are referenced to the modern elevations (NAVD88) that the paleotsunamis would have reached under modern sea level conditions. We add ±2 m uncertainty to all projected and adjusted shoreline inundation heights to address the uncertainties of storm surge (≤1.5 m; Peterson et al. 2008) and extreme tidal range (4 m, or ±2 m MSL; Mofjeld et al. 2004; Table 2). This uncertainty (±2 m NAVD88) is also expected to encompass minor surging and sand depletion in the terminal depositional settings of the selected run-up localities (Peterson et al. 2011).

The estimated shoreline inundation heights at the Crescent City and Elk Creek localities are 6–7 ± 2 m for event #1 and 13 ± 2 m for events #2 and #3 (Table 2; Fig. 6). The estimated shoreline inundation heights for events #3, #5 and event #6 or #7 at the Moore Creek and Beaver Creek localities are 15 ± 2 m. Estimated shoreline inundation heights at the Cannon Beach and Dawes Creek localities range from 7 ± 2 m (events #1 and #4) and 8 ± 2 m (events #2a and #2b) to 14 ± 2 m (events #3 and #5) (Table 2). Estimated shoreline inundation heights for the Waatch Creek and Sand Point localities range from 8–9 ± 2 m (events #1 and #2) to 11–12 ± 2 m (event #3). These projected shoreline inundation heights are similar to the recent tsunami inundation heights (10–15 m) reported for the open-coast settings of northeast Honshu, Japan, in 2011 (Mori et al. 2011; ITIC 2011). However, the central Cascadia paleotsunami run-ups are substantially smaller than the amplified run-ups (100–200 %) that were reported from the focused tsunami amplitude sites in deepwater bay-heads and abruptly narrowing alluvial valleys at Ogatsu Wan and Onagawa Wan in the Miyagi coastline (Lekkas et al. 2011). Unlike the deeply dissected and embayed Miyagi coastline of Japan, the central Cascadia paleotsunami sites used in this study occur in relatively straight coastline segments that are located landward of shallow broad inner shelves. None of the paleotsunami sand sheet deposit sites in Anchor Creek, Moore Creek, Dawes Creek or Sand Point (Fig. 3) occur in terminal valley pinch-outs where substantial flow amplification might be expected. Given the potential for some surge momentum or reflection at the proximal sites of the central Cascadia margin, it is important to note that none of the observed paleotsunami sand sheets (0.3–3.0 ka in age) exceeds 12.3 m in modern elevation (Table 2). There is no reported physical evidence of paleotsunami run-ups reaching 20–30 m along the central Cascadia margin.

4.3 Barrier overtopping estimates

Paleotsunami deposits mapped for maximum-recorded run-up at Neah Bay and Salt Creek (Fig. 1) are located on the landward sides of the protective beach barriers. We adjusted estimated shoreline inundation heights for event ages and relative sea level change (Table 2) to obtain values of 7–8 ± 2 m for events #1 and 2 and 9 ± 2 m for event #3 at Neah Bay and 3 ± 2 m for events #3 or #4 and event #5 at Salt Creek. The decrease in tsunami run-up amplitudes between Neah Bay and Salt Creek is consistent with numerically modeled tsunami run-up attenuation along the Juan de Fuca Strait (Cherniawsky et al. 2007).

Paleotsunami overtopping records at Catala and Kanim Lakes provide constraints on paleotsunami inundation heights at the northern Cascadia margin. Paleotsunami inundation heights at Catala Lake are estimated at ≥3 ± 2 and ≥2 ± 2 m, respectively, for events #1 and #3 based on (1) an overtopping elevation of 3 m (MSL) at the late outlet and (2) the regional rate of crustal uplift (1 m ka^{-1}; Table 2). We estimate a paleotsunami inundation height of ≥3±2 m for the single overtopping event (#5) at Kanim Lake, assuming (1) a modern lake outlet at 6-m MSL and (2) the regional rate of crustal uplift (−1 m ka^{-1}).

Subsequent paleotsunamis failed to overtop the rising outlet level at Kanim Lake, thereby limiting shoreline inundation heights to ≤4.3–4.9 ± 2 m between 1.7 and 1.1 ka, and ≤5.7 ± 2 m at 0.3 ka. Paleotsunami overtopping records from Kanim and Catala Lakes (0.3–4 ka in age) constrain adjusted shoreline inundation heights between 3 ± 2 and 6 ± 2 m MSL (Table 2; Fig. 5).

However, the adjusted paleotsunami shoreline inundation heights along the open coasts of Juan de Fuca Strait and the west coast of Vancouver Island (Fig. 1; Table 2) are not representative of potential tsunami run-up hazards in narrowed embayments and at fiord bay-heads along those coastlines. As many as ten paleotsunamis are recorded in marsh deposits (0–3 ka) at the terminal end of elongated Discovery Bay, WA, located 64 km east of Salt Creek (Fig. 1; Williams et al. 2005). And at least seven paleotsunami inundation events have been reported from the fiord bay-head delta deposits (0–3 ka) at Port Alberni, BC, 64 km form the open west coast of Vancouver Island (Clague and Bobrowsky 1994). In this paper, we do not evaluate the amplified paleotsunami run-up heights associated with

Table 3 Paleotsunami shoreline inundation heights, recurrence intervals and coseismic subsidence along the central Cascadia margin

Locality/event no.	Shoreline height (m)	Recurrence interval (ka)	Relative subsidence
Waatch			
#1	8 ± 2	0.8	Large
#2b	8 ± 2	0.2	Medium
#3	12 ± 2	0.4	Small
Sand Pt			
#3	11 ± 2	0.4	Small
Cannon			
#1	7 ± 2	0.8	Large
#2b	8 ± 2	0.2	Medium
#3	14 ± 2	0.4	Small
#4	7 ± 2	1.1	Large
Dawes			
#3	14 ± 2	0.4	Small
#5	14 ± 2	0.2	Small
Moore			
#1	8 ± 2	0.8	Large
#3	15 ± 2	0.4	Small
#4	7 ± 2	1.1	Large
#5	15 ± 2	0.2	Small
#6	15 ± 2	0.4	Small
Beaver			
#1	8 ± 2	0.8	Large
#2b	5 ± 2	0.2	Small
#3	15 ± 2	0.4	Small
#4	7 ± 2	1.1	Large
#5	14 ± 2	0.2	Small

Shoreline run-up data from Table 2. Recurrence interval data from Table 1. Relative subsidence data for Waatch/Sand (1) are extrapolated from Grays Harbor, WA; Cannon/Dawes (2) are from Willapa Bay, WA; Moore/Beaver (3) are extrapolated from Netarts Bay, OR (Fig. 1; Table 1)

narrowing deepwater embayments or fiord bay-head deltas along the glaciated coastlines of the northern Cascadia margin.

4.4 Along-margin variability of ocean shoreline run-ups

The average ocean shoreline inundation heights for the south, central and north Cascadia margin are, respectively, 10.5 ± 3.0 m ($N = 4$ samples), 10.0 ± 3.7 m ($N = 24$ samples) and 4 m ($N = 3$ samples). Shoreline inundation heights are largest on the central Cascadia margin at 15 ± 2 m (events # 3, #5 and #6). They decrease to 13 ± 2 m (events #2 and #3) on the southern Cascadia margin and to 4–5 ± 2 m (events # 1, #3 and # 5) on the northern Cascadia margin. Both the central and southern Cascadia margin localities record very modest run-up heights (~6–8 ± 2 m) for the last nearfield paleotsunami (event #1, AD 1700). How can this benchmark rupture event (M_w 9), with reported trans-Pacific manifestations in Japan (Satake et al. 1996, 2003), be reconciled with such modest near-field overland run-ups? This question is addressed in the section below.

4.5 Comparisons of event recurrence interval, relative coseismic subsidence and shoreline inundation heights

Shoreline inundation heights for events #1–6 are shown in Table 3, along with corresponding recurrence intervals and coseismic subsidence amounts. Coseismic subsidence on the landward side of the first zero-isobase should be proportional to, but smaller than, coseismic uplift on the seaward side of the first zero-isobase (Fig. 2). The magnitude of coseismic subsidence differs between events and between tidal marsh localities (Table 1) depending on coastal positions relative to the first zero-isobase.

Our results reveal that the largest paleotsunami run-ups and shoreline inundation heights (events #3 and #5) are associated with the shortest recurrence intervals between recorded regional coseismic subsidence events and smaller amounts of estimated coseismic subsidence (Table 3). The smallest recorded run-ups and corresponding shoreline inundation heights, correlated with events #1 and #4, correspond to the long recurrence intervals and to the largest amounts of coseismic subsidence, relative to the first zero-isobase (Peterson

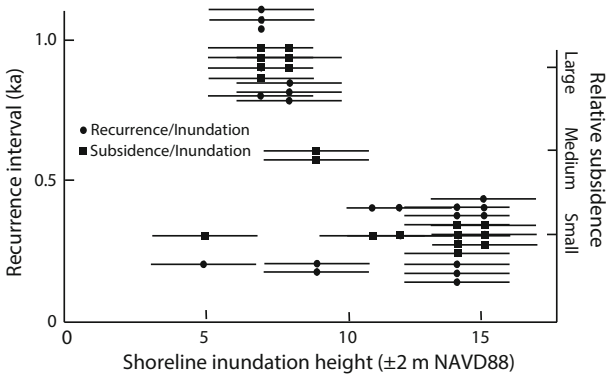

Fig. 7 *Plots* of shoreline inundation height (±2 m NAVD88), recurrence interval (ka) and relative coseismic subsidence (large, medium, small) for rupture events #1–6 on the central Cascadia margin. All data are from Table 3

and Cruikshank 2014). These results are contrary to expected results from dislocation-fit modeling of tsunami excitation.

Predictions of tsunami excitation by dislocation modeling are based on assumptions that tsunami amplitude is proportional to the release of elastic vertical strain that accumulated in the upper plate during the preceding interseismic interval (Geist 1999). The results from this study, however, show little or no relation between measured deposit run-up elevations or projected shoreline inundation heights and (1) the length of the preceding interval between coseismic subsidence events (Table 1; Fig. 2) or (2) the amount of coseismic subsidence relative to the first zero-isobase (Fig. 7). These results call into question some of the assumptions used in dislocation-fit modeling of tsunami excitation along the central Cascadia margin (Geist 2005; Priest et al. 2010; Witter et al. 2013). Possible explanations for the lack of agreement between field evidence and model assumptions are (1) latent strain was not released during previous megathrust ruptures, (2) near-surface thrust faulting in the upper plate accompanied megathrust ruptures, (3) non-tsunamigenic slip preceded megathrust ruptures, and/or (4) offshore vertical strain release is not represented by onshore coseismic subsidence.

The uncertainty in megathrust rupture mechanics along the central Cascadia margin is shown by paleotsunami event #2a at 0.8–0.9 ka (Table 2). This event lacks any reports of coeval coastal coseismic subsidence in southwest Washington or northwest Oregon (Table 1), although it is regionally represented by a paleotsunami in the northern half of the central Cascadia margin (Table 2) and by offshore turbidite records along the length of the margin (Atwater and Griggs 2012). The lack of apparent coastal coseismic subsidence argues against release of regional elastic vertical strain during this event, as does the discontinuation of major paleotsunami deposition from this event on the southern half of the central Cascadia margin (Peterson and Darienzo 1996; Peterson et al. 2011). Should we assume that this event released the elastic vertical strain accumulated between 1.1 and $\sim$0.85 ka even though there is little or no record of coseismic subsidence, and if so, then along what portions of the Cascadia margin was it released? Even if this event did reset elastic strain accumulation after $\sim$0.85 ka throughout the central Cascadia margin, what accounts for the relatively modest estimated run-ups (6–8 $\pm$ 2 m) estimated for the AD1700 paleotsunami (Table 2), which would have had a relatively long preceding elastic strain interval of at least 550 years? Much more empirical evidence is needed to constrain the areal extents and amplitudes of tsunamigenic seafloor displacements that are predicted by numerically modeled rupture scenarios.

Future tsunami inundation maps of the Cascadia margin should be based on regional tsunami inundation models that are calibrated to, or independently verified by, established paleotsunami run-up records and/or estimated shoreline inundation heights determined at reliable calibration localities. For purposes of evacuation planning in the central Cascadia margin, the relatively short interseismic period since the last Cascadia rupture (0.3 ka) should not be assumed to yield smaller tsunami run-ups for a near-future event, as predicted by current dislocation-fit tsunami excitation modeling. Instead the coastal communities need to plan for the maximum-recorded run-ups established from the paleotsunami records at nearest corresponding paleotsunami calibration localities (Fig. 6; Table 3). The calibration of model simulations by paleotsunami run-up records in Honshu, Japan, might have led to greater predicted run-ups, prior to the 2011 Tohoku-Oki earthquake tsunami (Ando et al. 2011; Satake et al. 2013; Sugawara et al. 2013). The use of paleotsunami run-up measurements based on maximum elevations and landward extents of preserved sand sheets might underestimate flooding distances in some low-gradient settings. Nevertheless, numerical model verification by paleotsunami deposit data should (1)

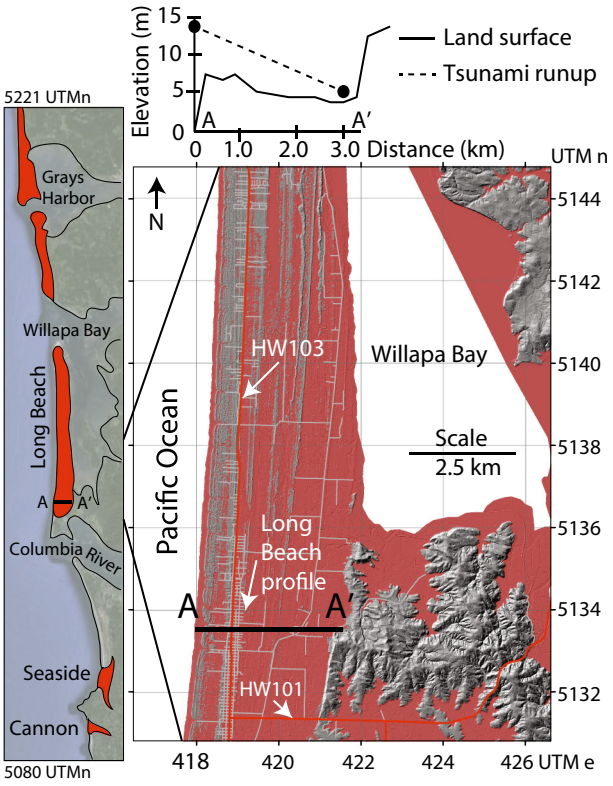

Fig. 8 *Left* map of low-elevation barrier spits and beach plains (*red*) at approximately 4- to 7-m elevation (NAVD88) in south-central Washington and northernmost Oregon (Fig. 1). *Top* predicted tsunami height based on a 14-m shoreline inundation height and a landward -3 m km^{-1} elevation attenuation gradient (*dashed line*) across the spit land surface (*solid line*) at the south end of the Long Beach peninsula. *Right* predicted tsunami inundation of the low-elevation (<6.5 m) barrier spit (*red* and *low-contrast gray*) at Long Beach. *Low-contrast gray* areas (6.5- to 9-m elevation) are abandoned foredune ridges and buildings in beachfront communities. *High-contrast gray* areas are high terraces. Evacuation routes (3–7 km distance from beach front communities) include narrow roads (*thin gray lines*) and two highways (*red lines*: HW103 and HW101)

confirm high-impact zones of high-velocity flooding, (2) increase the publics' confidence about the predicted tsunami hazards and (3) help to motivate expenditures for dedicated evacuation routes and/or vertical evacuation structures in the most at-risk communities (Peterson et al. 2013a).

4.6 Example application of maximum projected tsunami run-up elevations

Plans for evacuating at-risk populations during the next Cascadia megathrust rupture and tsunami have progressed slowly in many coastal communities in the Pacific Northwest after tsunami evacuation signposts were first installed more than a decade ago. Tsunami surges could arrive in many coastal communities within 15–20 min of the strong ground shaking from a megathrust earthquake (Meyers 1994). Of particular concern are low-lying beach plains in southwest Washington and northern Oregon (Walsh et al. 2000). In this article, we use the estimated maximum shoreline inundation height of 14 $\pm$ 2 m in Cannon

Beach and the empirical flow height attenuation gradient of -3 m km^{-1} to show that the south end of the Long Beach barrier spit at Willapa Bay could be inundated by high-velocity tsunami waves shortly after a megathrust earthquake (Fig. 8). The full width (3.0 km) of the south end of the barrier spit could be flooded by a 14-m run-up event. Is planned evacuation to elevated terraces at 3–7 km distance from the beachfront communities practical? Narrow unimproved roads that cross the wetland bogs east of the beachfront communities might not be suitable for mass evacuations of mixed vehicle and pedestrian traffic. Pedestrian evacuation over distances of 3–7 km within 20 min of a great earthquake might not be possible, particularly for children and seniors, and especially at night, or due to delayed evacuation warnings. Based on the tsunami hazard conditions summarized above, additional night-lighted pedestrian evacuation routes to vertical evacuation structures are warranted in low-elevation beach plain settings that lack suitable high-ground evacuation options.

5 Conclusions

In this study, we compile maximum-recorded run-up data for major nearfield paleotsunamis at the Cascadia subduction zone over the past 3 ka. The run-up data are derived from reported landward extents and elevations of terminal paleotsunami sand or gravel sheets. In this study, the extents of terminal sand sheets are (1) projected to the coastline using terminal deposit elevations and inland distances, and an empirical paleotsunami deposit height–distance gradient of 3 m km^{-1} and (2) adjusted to the modern elevation datum (NAVD88) based on paleotsunami ages and relative sea level curves. The resulting shoreline inundation heights for the largest paleotsunamis range from 11 to 12 $\pm$ 2 m in northernmost Washington to 14 $\pm$ 2 m near the Washington–Oregon border, to 15 $\pm$ 2 m in central Oregon, and 13 $\pm$ 2 m near the Oregon–California border. Smaller adjusted run-ups are estimated for open-coast shorelines along Vancouver Island (3–5 $\pm$ 2 m) and the east end of Juan de Fuca Strait (2–3 $\pm$ 2 m).

The two largest paleotsunami on the central Cascadia margin occurred during great earthquakes with relatively short recurrence intervals (200–400 year) between dated coseismic subsidence events. The last Cascadia megathrust rupture ($\sim M_w$ 9) occurred 300 years ago, after a long recurrence interval (either 800 or $\sim$550 year), but it resulted in modest shoreline inundations (run-up heights of 6–8 $\pm$ 2 m). The extents of paleotsunami sand sheets compiled in this study represent high-velocity flows, so they likely underestimate maximum flooding elevations and distances. Nevertheless, the reported terminal sand sheet deposits can be used to calibrate or validate modeled tsunami excitation along the Cascadia margin. Broad low-elevation barriers and beach plains in northernmost Oregon and southwest Washington, which have surface elevations of 4–7 m, are particularly susceptible to inundation by tsunamis with shoreline inundation heights of up to 14–15 $\pm$ 2 m, as estimated for the central region of the study area.

References

Abramson H (1998) Evidence for tsunami and earthquakes during the last 3500 years from Lagoon Creek, a coastal freshwater marsh, northern California. MSc thesis, Humboldt State University, Arcata, CA, p 75

Adams J (1996) Great earthquakes recorded by turbidites off the Oregon–Washington coast. In: Rogers AM, Walsh TJ, Kockelman WJ, and Priest GR (eds), US Geol Surv Prof Pap 1560, pp 147–158
Ando M, Ishida M, Hayashi Y, Mizuki C (2011) Interviews with survivors of Tohoku earthquake provide new insights into fatality rate. Forum, EOS Trans Am Geophys Union 92:411–412
Andrade MJ (1931) Quileute texts. Columbia Univ Contribution Anthropol 12, New York. Reprinted 1969 AMS Press, New York
Atwater BF, Griggs GB (2012) Deep-sea turbidites as guides to Holocene earthquake history at the Cascadia Subduction Zone—Alternative views for a seismic-hazard workshop. U.S. Geol Surv Open-File Rep 2012–1043
Atwater BF, Hemphill-Haley E (1997) Recurrence intervals for great earthquakes of the past 3500 years at northeastern Willapa Bay, Washington. US Geol Surv Prof Pap 1576:108
Atwater BF, Tuttle MP, Schweig ES, Rubin CM, Yamaguchi DK, Hemphill-Haley E (2004) Earthquake recurrence, inferred from paleoseismology. In: Gillespie AR, Porter SC, Atwater BF (eds) The quaternary period in the United States. Elsevier, Amsterdam, pp 331–350
Carver DH (1988) Native stories of earthquake and tsunamis Redwood National Park, California. National Park Service Redwood National and State Parks, Arcata, California
Carver GA, Abramson HA, Garrison-Laney CE, Leroy T (1998) Investigation of paleotsunami evidence along the north coast of California. Unpublished report prepared for Pacific Gas and Electric Co, San Francisco, CA, p 167 and appendix
Carver GA, Abramson HA, Garrison-Laney CE, Leroy T (1999) Paleotsunami evidence from northern California for repeated long rupture (M 9) of the Cascadia subduction zone. Sesimol Res Lett 20(2):232
Cherniawsky JY, Titov VV, Wang K, Li JY (2007) Numerical simulations of tsunami waves and currents for southern Vancouver Island from a Cascadia megathrust earthquake. Pure appl Geophys 164:465–492
Clague JJ, Bobrowsky PT (1994) Tsunami deposits beneath tidal marshes on Vancouver Island, British Columbia. Geol Soc Amer Bull 106:1293–1303
Clague JJ, Hutchinson I, Mathewes RW, Patterson RT (1999) Evidence for late holocene tsunamis at Catala Lake, British Columbia. J Coastal Res 15:45–60
Clague JJ, Bobrowsky PT, Hutchinson I (2000) A review of geological records of large tsunamis at Vancouver Island, British Columbia, and implications for hazard. Quat Sci Rev 19:849–863
Darienzo ME, Peterson CD, Clough C (1994) Stratigraphic evidence for great subduction zone earthquakes at four estuaries in northern Oregon. J Coastal Res 10:850–876
Garrison-Laney CE (1998) Diatom evidence for tsunami inundation from Lagoon Creek, a coastal freshwater pond, Del Norte County, California. MSc thesis, Humboldt State University, Arcata, CA, p 97
Geist EL (1999) Local tsunamis and earthquake source parameters. Adv Geophys 39:117–209
Geist EL (2005) Local tsunami hazards in the Pacific Northwest from Cascadia subduction zone earthquakes. US Dept Int, US Geol Surv, Reston, VA
Geist E, Yoshioka S (1996) Source parameters controlling the generation and propagation of potential local tsunamis along the Cascadia margin. Nat Hazards 13(2):151–177
Goff J, Chague-Goff C, Nichol S, Jaffe B, Dominey-Howes D (2012) Progress in paleotsunami research. Sed Geol 243–244:70–88
Goto K, Imamura F, Keerthi N, Kunthasap P, Matsui T, Minoura K, Ruangrassamee A, Sugawara D, Supharatid S (2008) Distributions and significances of the 2004 Indian Ocean tsunami deposits—initial results from Thailand and Sri Lanka. Tsunamiites Featur Implic. Elsevier, Amsterdam, pp 105–122
Hawkes AD, Bird M, Cowie S, Grundy-Warr C, Horton BP, Hwai ATS, Law L, Macgregor C, Nott J, Ong JE, Rigg J, Robinson R, Tan-Mullins M, Sa TT, Yasin Z, Aik LW (2007) Sediments deposited by the 2004 Indian Ocean tsunami along the Malaysia–Thailand peninsula. Mar Geol 242:169–190
Hutchinson I, Clague JJ, Rolf Mathewes RW (1997) Reconstructing the tsunami record on an emerging coast: a case study of Kanim Lake, Vancouver Island, British Columbia, Canada. J Coastal Res 13:545–553
Hutchinson I, Guilbault JP, Clague JJ, Bobrowsky PT (2000) Tsunamis and tectonic deformation at the northern Cascadia margin: a 3000-year record from Deserted Lake, Vancouver Island, British Columbia. Holocene 10:429–439
Hutchinson I, Peterson CD, Sterling S (2013) Late Holocene tsunami deposits at Salt Creek, Washington, USA. Sci Tsunami Hazards 32:221–235
ITIC (2011) International Tsunami Information Centre tsunami newsletter. Gt East Jpn Earthq XLIII(1):1–15
James TS, Clague JJ, Wang K, Hutchinson I (2000) Postglacial rebound at the northern Cascadia subduction zone. Quat Sci Rev 19:1527–1541

Kelsey HM, Nelson AR, Hemphill-Haley E, Witter RC (2005) Tsunami history of an Oregon coastal lake reveals a 4600 yr record of great earthquakes on the Cascadia subduction zone. Geol Soc Am Bull 117:1009–1032

Landers JF, Lockridge PA, Kozuch MJ (1993) Tsunami affecting the west coast of the United States 1806–1992. US Dep Comm Tech Rep, NGDC key to geophys records documentation no 29,p 242

Lekkas E, Andreadakis E, Kostaki I, Kapourani E (2011) Critical factors for run-up and impact of the Tohoku earthquake tsunami. Intern J Geosci 2:310–317

Ludwin RS, Dennis R, Carver D, McMillan AD, Losey R, Clague J, Jonientz-Trisler C, Bowechop J, Wray J, James K (2005) Dating the 1700 Cascadia earthquake: great coastal earthquakes in Native stories. Seismol Res Lett 76:140–148

Meyers EP (1994) Numerical modeling of tsunamis with applications to the Sea of Japan and the Pacific Northwest. MSc thesis, Oregon Graduate Inst Sci Tech, Beaverton, OR, p 161

Minoura K, Nakaya S (1991) Traces of tsunami preserved in inter-tidal lacustrine and marsh deposits: some examples from northeast Japan. J Geol 99:265–287

Minoura KF, Imamura D, Sugawara Y, Kono Iwashita T (2001) The 869 Jogan tsunami deposit and recurrence interval of large-scale tsunami on the Pacific coast of northeast Japan. J Nat Disaster Sci 23:83–88

Mofjeld HO, Venturato AJ, González FI, Titov VV (2004). Background tides and sea level variations at Seaside, Oregon. National Oceanic and Atmospheric Memorandum OAR PMEL-126. Pac Mar Environ Lab, Seattle, WA, Contribution 2736, p 15. www.pmel.noaa.gov/pubs/PDF/mofj2736/mofj2736.pdf. Accessed 22 Feb 2015

Mori N, Takahashi T, Yasuda T, Yanagisawa H (2011) Survey of 2011 Tohoku earthquake tsunami inundation and run-up. Geophys Res Lett 38(7):L00G14. doi:10.1029/2011GL049210

Ng MKF, Leblond PH, Murty TS (1990) Simulation of tsunamis from great earthquakes on the Cascadia subduction zone. Science 250:1248–1251

Osamu F, Kenkyu D (2007) Major contribution of tsunami deposit studies to Quaternary research. Quat Res 46:293–302

Peters R, Jaffe B, Gelfenbaum G (2007) Distribution and sedimentary characteristics of tsunami deposits along the Cascadia margin of western North America. Sed Geol 200(3):372–386

Peterson CD, Cruikshank KM (2011) Proximal records of paleotsunami run-up in barrage creek floodplains from late-Holocene great earthquakes in the Central Cascadia Subduction Zone, Oregon, USA. In: Mokhtari M (ed), Tsunami a growing disaster. InTec. http://www.intechopen.com/articles/show/title/proximal-records-of-paleotsunami-run–up-in-barrage-creek-floodplains-from-late-holocene-great-earthquakes

Peterson CD, Cruikshank KM (2014) Quaternary tectonic deformation, Holocene paleoseismicity, and modern strain in the unusually-wide coupled zone of the central Cascadia margin, Washington and Oregon, USA and British Columbia, Canada. J Geogr Geol 6:1–33

Peterson CD, Darienzo ME (1996) Discrimination of flood, storm and tectonic subsidence events in coastal marsh records of Alsea Bay, Central Cascadia Margin, USA. In: Rogers AM, Walsh TJ, Kockelman WJ, Priest GR (eds), Assessing and reducing earthquake hazards in the Pacific Northwest. US Geol Surv Prof Pap 1560(1):115–146

Peterson CD, Darienzo ME, Pettit DJ, Jackson P, Rosenfeld C (1991) Littoral cell development in the convergent Cascadia margin of the Pacific Northwest, USA. In: Osborne R (ed.), From shoreline to the abyss, contributions in marine geology in honor of F. P. Shepard. SEPM Spec Pub 46: 17–34

Peterson CD, Doyle DL, Barnett ET (2000) Coastal flooding and beach retreat form coseismic subsidence in the central Cascadia margin, US. Environ Eng Geosci 6:255–269

Peterson CD, Cruikshank KM, Jol HM, Schlichting RB (2008) Minimum run-up heights of paleotsunami from evidence of sand ridge overtopping at Cannon Beach, Oregon, central Cascadia margin, USA. J Sed Res 78:390–409

Peterson CD, Cruikshank KM, Schlichting RB, Braunsten S (2009) Distal run-up records of latest Holocene paleotsunami inundation in alluvial flood plains: Neskowin and Beaver Creek, Oregon, central Cascadia margin, USA. J Coastal Res 26:622–634

Peterson CD, Jol HM, Horning T, Cruikshank KM (2010) Paleotsunami inundation of a beach ridge plain: cobble ridge overtopping and inter-ridge valley flooding in Seaside, Oregon, USA. J Geol Res 276989:22. doi:10.1155/2010/276989

Peterson C, Carver G, Cruikshank K, Abramson H, Garrison-Laney C, Dengler L (2011) Evaluation of the use of paleotsunami deposits to reconstruct inundation distance and run-up heights associated with prehistoric inundation events, Crescent City, southern Cascadia margin. Earth Surf Proc Landf 36:967–980

Peterson CD, Clague JJ, Carver GA, Cruikshank KM (2013a) Recurrence intervals of major paleotsunamis as calibrated by historic tsunami deposits in three localities: Port Alberni, Cannon Beach, and Crescent City, along the Cascadia margin, Canada and USA. Nat Hazards 68:321–336

Peterson CD, Cruikshank KM, Darienzo ME, Wessen G, Butler V, Sterling S (2013b) Coseismic subsidence and paleotsunami run-up records from latest Holocene deposits in the Waatch Valley, Neah Bay, northwest Washington, USA: links to great earthquakes in the northern Cascadia margin. J Coastal Res 29:157–172

Peterson CD, Butler VL, Feathers JK, Cruikshank KM (2014) Geologic records of net littoral drift, beach plain development, and paleotsunami runup, North Sand Point, Olympic Peninsula, Washington, USA. Northwest Sci 88:314–328

Phillips PW (2007) Tsunamis and floods in Coos Bay mythology. great Cascadia earthquakes and tsunamis. Oregon Hist Quart 108:180–192

Priest GR, Myers E, Baptista AM, Fleuck P, Wang K, Peterson CD (2000) Source simulation for tsunamis: lessons learned from fault rupture modeling of the Cascadia subduction zone, North America. Sci Tsunami Hazards 18:77–106

Priest GR, Goldfinger C, Wang K, Witter RC, Zhang Y, Baptista AM (2010) Confidence levels for tsunami-inundation limits in northern Oregon inferred from a 10,000-year history of great earthquakes at the Cascadia subduction zone. Nat Hazards 54:27–73

Priest GR, Witter RC, Zhang YJ, Wang K, Goldfinger C, Stimely LL, English JT, Pckner SG, Hughes, KLB, Wille TE, Smith RL (2013) Tsunami inundation scenarios for Oregon. Open-file report 0-13-19. Oregon Dept Geol Min Ind, Portland, OR

Satake K, Shimazaki K, Tsuji Y, Ueda K (1996) Time and size of giant earthquake in Cascadia inferred from Japanese tsunami records of January 1700. Nature 378:246–249

Satake K, Wang K, Atwater BF (2003) Fault slip and seismic moment of the 1700 Cascadia earthquake inferred from Japanese tsunami descriptions. J Geophys Res, Solid Earth 108(B11):2535. doi:10.1029/2003JB002521

Satake K, Fujii Y, Harada T, Namegaya Y (2013) Time and space distribution of coseismic slip of the 2011 Tohoku earthquake as inferred from tsunami waveform data. Bull Seismol Soc Amer 103:1473–1492

Schlichting RB, Peterson CD (2006) Mapped overland distance of paleotsunami high-velocity inundation in back-barrier wetlands of the central Cascadia margin, USA. J Geol 114:577–592

Shennan I, Long A, Rutherford M, Green F, Innes J, Loyd J, Zong Y, Walker K (1996) Tidal marsh stratigraphy, sea-level change, and large earthquakes, 5000 year record of large earthquakes in Washington, USA. Quat Sci Rev 15:1023–1059

Sproat GM, Lillard C (1987) The Nootka: scenes and studies of savage life. Sono Nis Press, Victoria

Sugawara D, Imamura F, Goto K, Matsumoto H, Minoura K (2013) The 2011 Tohoku-oki earthquake tsunami: similarities and differences to the 869 Jogan tsunami on the Sendai plain. Pure appl Geophys 170:831–843

Swan JG (1870) The Indians of Cape Flattery, at the Entrance to the Strait of Juan Fuca, Washington Territory. Smithsonian Contrib Knowledge 16. Smithsonian Inst, Washington DC

Tsunami Pilot Study Working Group (2006) Seaside, oregon tsunami pilot study-modernization of FEMA flood hazard maps. NOAA OAR Spec Rep, NOAA/OAR/PMEL, Seattle, WA, p 94

Uslu B, Borrero JC, Dengler LA, Synolakis CE (2007) Tsunami inundation at Crescent City generated by earthquakes along the Cascadia Subduction Zone. Geophys Res Lett 34:L20601. doi:10.1029/2007GL030188

Walsh TJ, Caruthers CG, Heinitz AC, Baptista AM, Kamphaus RA (2000) Tsunami hazard map of the southern Washington coast: modeled tsunami inundation from a Cascadia subduction zone earthquake. Wash Div Geol Earth Resour, Olympia, WA, Geol Map GM-49

Whitmore PM (1993) Expected tsunami amplitudes and currents along the North American coast for Cascadia subduction zone earthquakes. Nat Hazards 8:59–73

Whitmore PM (1994) Expected tsunami amplitudes off the Tillamook County, Oregon coast, following a major Cascadia subduction zone earthquake. Oregon Geol 56:62–64

Williams HFL, Hutchinson I, Nelson AR (2005) Multiple sources for late-Holocene tsunamis at Discovery Bay, Washington Sate, USA. Holocene 15:60–73

Witter RC, Zhang YJ, Wang E, Priest GR, Goldfinger C, Stimely L, English JT, Ferro PA (2013) Simulated tsunami inundation for range of Cascadia earthquake scenarios at Bandon, Oregon, USA. Geosphere. doi:10.1130/GES00899.1

Younker JT (2007) Weaving long ropes. Great Cascadia earthquakes and tsunamis. Oregon Hist Quart 108:193–201